Electronic Transactions on Numerical Analysis.
Volume 38, pp. 258-274, 2011.

ISSN 1068-9613.

ETNA
Kent State University
http://etna.math.kent.edu

APPLICATION OF BARYCENTER REFINED MESHES IN LINEAR ELASTICITY AND INCOMPRESSIBLE FLUID DYNAMICS*

MAXIM A. OLSHANSKII† AND LEO G. REBHOLZ‡

Abstract. The paper demonstrates that enhanced stability properties of some finite element methods on barycenter refined meshes enables efficient numerical treatment of problems involving incompressible or nearly incompressible media. One example is the linear elasticity problem in a pure displacement formulation, where a lower order finite element method is studied which is optimal order accurate and robust with respect to the Poisson ratio parameter. Another example is a penalty method for incompressible viscous flows. In this case, we show that barycenter refined meshes prompt a "first penalize, then discretize" approach, avoiding locking phenomena, and leading to a method with optimal convergence rates independent of the penalty parameter, and resulting in discrete systems with advantageous algebraic properties.

Key words. finite element method, barycenter-mesh refinement, locking-free penalty method, Navier-Stokes equations, linear elasticity

AMS subject classifications. 65F05, 65M60, 65M12, 76D05, 74B05

1. Introduction. This article shows that, provided a mild mesh restriction that is simple to implement using triangular or tetrahedral elements, optimal accuracy can be achieved in finite element methods for both the classical penalty method of Temam for the incompressible Navier-Stokes equations (NSE) using only the velocity variable [22, 38, 39], and the pure displacement formulation of linear elasticity problems for nearly incompressible media [11]. For both of these problems, locking phenomena and suboptimal accuracy can occur if care is not taken in the element choice, and in some cases, the integration accuracy may need to be reduced. For commonly used triangular/tetrahedral elements, however, no simple, practical, efficient, and optimally accurate method seems to exist, and it is the goal of this work to derive such a method.

It has been known for some time that the Scott-Vogelius (SV) pair $\{(P_k)^d, P_{k-1}^{disc}\}$ ($d = 2$ or 3 is the space dimension) is an LBB stable Stokes element on the barycenter refined meshes provided that $k \geq d$ [2, 42] (see Figure 1.1 for an example of a barycenter refinement). Since $(\mathrm{div}\,(P_k)^d) \subset P_{k-1}^{disc}$, it is an example of a stable element which enforces pointwise the divergence free constraint for the velocity. Recently, this element was extensively applied to solving those problems where numerical mass conservation is critical [12, 29]. One consequence of pointwise mass conservation and inf-sup stability of the element is that an arbitrarily large penalization of the divergence constraint for *any* $(P_k)^d$-based element on barycenter refined meshes does not lead to overstabilization or locking phenomena, regardless of the supplementing pressure space (and in particular it holds for any of the velocity-pressure pairs $((P_k)^d, P_{k-1})$, $((P_k)^d, P_{k-2})$, $\dots((P_k)^d, \{0\})$). This property has been noticed and exploited for various flow problems with Taylor-Hood (TH) finite elements in [8, 12]. In the present paper we show that in the limit case of zero pressure space, this approach is closely related to methods which eliminate or avoid introducing a pressure variable, such as the penalty method for incompressible flow problems and the solution of the linear elasticity problem in a pure displacement formulation.

*Received February 17, 2011. Accepted for publication September 14, 2011. Published online October 5, 2011 Recommended by A. Klawonn.

†Department of Mechanics and Mathematics, Moscow State M. V. Lomonosov University, Moscow 119899, Russia; Maxim.Olshanskii@mtu-net.ru, partially supported by the RFBR Grants 08-01-00415 and 09-01-00115.

‡Department of Mathematical Sciences, Clemson University, Clemson, SC 29634, rebholz@clemson.edu, http://www.math.clemson.edu/∼rebholz, partially supported by the National Science Foundation grant DMS0914478.

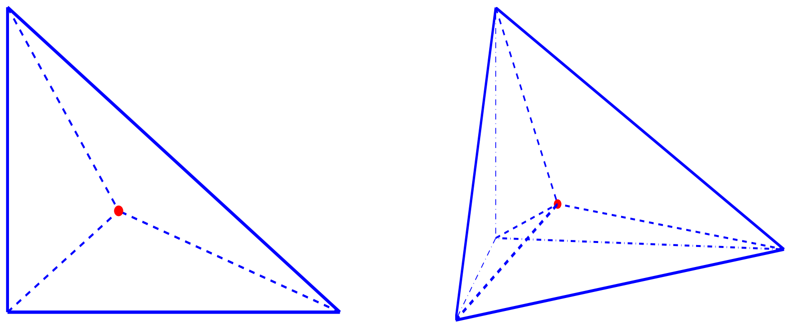

FIG. 1.1. *Shown above is a barycenter refinement of a triangle and a tetrahedra.*

Numerically solving the linear elasticity problem is known to be difficult as the media becomes nearly incompressible [11]. In such cases, numerical solutions are forced into a (nearly) divergence free subspace of the discrete solution space, which can lead to poor approximations and even locking phenomena. However, if the pure displacement form is used with solution space $X_h = (P_k)^d$ on a barycenter refined mesh and $k \geq d$, the divergence free subspace of X_h is guaranteed to retain optimal approximation properties. Thus in this setting, optimal accuracy can be expected for nearly incompressible media. In Section 2, we expand this idea and provide a numerical example demonstrating its effectiveness.

The second problem studied herein is for the Navier-Stokes equations of an incompressible viscous fluid, which couple pressure and velocity variables, and possess well-known numerical stability issues and algorithmic challenges, e.g., [19, 20, 26, 40]. The formal decoupling is not possible due to the incompressibility constraint except in some very special cases. Several ways of numerical decoupling have been suggested in the literature and successfully used for practical computations, including artificial compressibility, pseudo-compressibility, penalty and projection methods, e.g., [13, 14]. The penalty method for the Navier-Stokes system was introduced by Temam in [38, 39]: Given a (small) penalty parameter ε one looks for a solution $\mathbf{u}^\varepsilon, p^\varepsilon$ to

$$(1.1)\qquad \begin{cases} \mathbf{u}_t^\varepsilon - \nu\Delta\mathbf{u}^\varepsilon + (\mathbf{u}^\varepsilon\cdot\nabla)\mathbf{u}^\varepsilon + \frac{1}{2}(\operatorname{div}\mathbf{u}^\varepsilon)\mathbf{u}^\varepsilon + \nabla p^\varepsilon = \mathbf{f}, \\ \operatorname{div}\mathbf{u}^\varepsilon + \varepsilon p^\varepsilon = 0, \quad \mathbf{u}^\varepsilon|_{t=0} = \mathbf{u}^0. \end{cases}$$

The pressure may be eliminated from the system (1.1), resulting in

$$(1.2)\qquad \mathbf{u}_t^\varepsilon - \nu\Delta\mathbf{u}^\varepsilon + (\mathbf{u}^\varepsilon\cdot\nabla)\mathbf{u}^\varepsilon + \frac{1}{2}(\operatorname{div}\mathbf{u}^\varepsilon)\mathbf{u}^\varepsilon - \varepsilon^{-1}\nabla\operatorname{div}\mathbf{u}^\varepsilon = \mathbf{f}, \quad \mathbf{u}^\varepsilon|_{t=0} = \mathbf{u}^0.$$

The method was further studied in the literature, see, e.g., [9, 16, 19, 21, 27, 31, 36]. In particular, $O(\varepsilon)$ convergence of $\mathbf{u}^\varepsilon, p^\varepsilon$ to the Navier-Stokes solution $\mathbf{u}, p$ was proved in [36]:

$$(1.3)\qquad \begin{aligned} &\sqrt{t}\|\mathbf{u}(t)-\mathbf{u}_\varepsilon(t)\| + \sqrt{\nu}t\|\nabla(\mathbf{u}(t)-\mathbf{u}_\varepsilon(t))\| \\ &\qquad + \left(\int_0^t s^2\|p(s)-p_\varepsilon(s)\|^2\mathrm{d}s\right)^{\frac{1}{2}} \leq C\varepsilon, \forall t\in(0,T]. \end{aligned}$$

Although the approach is straightforward, simple, and enjoys a solid mathematical justification it has not received as much attention as artificial compressibility and projection methods by practitioners. The likely reason is the following shortcomings of the method: For small values of ε, a Galerkin finite element method applied to (1.2) may lead to a locking phenomena similar to that of the elasticity problem. Moreover, small values of ε make the algebraic system ill conditioned, since it is dominated by the $\varepsilon^{-1}\nabla\mathrm{div}$ type term with possibly large non-trivial kernel. The latter leads to poor convergence of most of available iterative solvers, prompting us to look for a direct solvers/factorizations rather than iterative. We point, however, to papers [6, 15, 35], where special multigrid and domain decomposition methods show promising results in certain cases. Otherwise, the question of efficient algebraic solvers for discrete velocity system, resulting after elimination of pressure, seems to be largely overlooked in the literature.

The natural way around the first difficulty would be first to discretize (1.1) and then to eliminate pressure from the discrete system. In this case locking does not occur for small values of ε, however, the choice of an efficient algebraic solver remains problematic. In particular, it is shown in [7] that at least for certain finite element pairs this "first discretize, then eliminate" approach leads to algebraic systems with (significantly) larger fill-in patterns than direct discretization of (1.2), thus making algebraic solvers significantly more expensive.

In the recent paper [31] it is proved that the specific choice of the Crouzeix-Raviart nonconforming P1 finite element leads to optimal order ε-independent convergence if applied directly to (1.2) (i.e., "first penalize then eliminate and discretize" approach). In the present paper we show that with barycenter refined meshes and $k \geq d$, direct discretizations of (1.2) will provide optimal accuracy (no locking or overstabilization) and keep the sparsity structure of matrices reasonable for direct solvers to be successful. Thus, the paper extends the results of [31] to higher order and conforming finite elements. We also provide the computational evidence of the effectiveness and reliability of the approach by considering several standard 2D and 3D benchmark problems.

We note that on general triangular/tetrahedral meshes, LBB stability of SV elements is not known to be LBB unless $k \geq 2d$ [2, 44] , which is a prohibitive restriction. To use smaller k, special types of meshes that allow the correct ratio of the local sizes of the velocity and pressure spaces, can be shown to satisfy LBB by following arguments of Stenberg [37]. To our knowledge, the barycenter refined mesh is the simplest type of mesh where LBB holds for 'reasonable' k. With this mesh condition, however, comes some mild restrictions. The minimum angle of the pre-refined mesh will be cut in half, and so the pre-refined mesh must have a large minimum angle condition to avoid 'flat' elements after the barycenter refinement is applied. Also, mesh refinement must be performed more carefully than usual by first refining the coarser (non-barycenter refined) mesh, and then applying a barycenter refinement. The ideas presented in this work can be extended to $k < d$ if somewhat more elaborate (and more restrictive) meshes are used; for example, $k = 2,\ d = 3$ and $k = 1,\ d = 2$ are possible choices provided meshes with appropriate macro-element structure are chosen [43, 45].

The remainder of the paper is organized as follows. In section 2, we study the linear elasticity problem in displacement formulation with barycenter meshes. Here we find optimal accuracy can be achieved and provide numerical evidence of it, and that on general meshes accuracy is suboptimal. Section 3 applies the methodology to the incompressible, viscous Navier-Stokes equations, and several numerical experiments are given that demonstrate both the efficiency and accuracy of the proposed method.

2. Application to linear elasticity. Consider the linear elasticity problem, written in displacement variables,

$$-2\mu\,\mathbf{div}\,D(\mathbf{u}) - \frac{\nu}{1-2\nu}\nabla(\operatorname{div}\mathbf{u}) = \mathbf{f} \quad \text{in} \quad \Omega, \tag{2.1}$$

$$\mathbf{u} = \mathbf{g} \quad \text{on} \quad \partial\Omega, \tag{2.2}$$

where $\mathbf{u}$ is the displacement, $\mathbf{f}$ is the body force, $D(\mathbf{u})$ is the strain (deformation) tensor, $\mathbf{g}$ is the Dirichlet boundary condition (results can easily be extended to other common boundary conditions), ν denotes Poisson's ratio and μ is the shear modulus given by

$$\mu = \frac{E}{2(1+\nu)},$$

where E is Young's modulus. Of particular interest is nearly-incompressible media, when the Poisson ratio $\nu \approx 0.5$. In this case, although it is known that the problem (2.1) and (2.2) is well-posed for all $0 \leq \nu < 0.5$ [1], standard methods often fail or provide sub-optimal accuracy [11, 17]. Consider the standard finite element formulation of (2.1)and (2.2), where for simplicity $\mathbf{g} = \mathbf{0}$, and $\gamma := \frac{\nu}{1-2\nu}$ (so of interest is now $\gamma \to \infty$): Find $\mathbf{u}_h \in X_h \subset (H_0^1(\Omega))^d$ satisfying

$$2\mu(D(\mathbf{u}_h), D(\mathbf{v}_h)) + \gamma(\mathrm{div}\,\mathbf{u}_h, \mathrm{div}\,\mathbf{v}_h) = (\mathbf{f}, \mathbf{v}_h), \;\; \forall\, \mathbf{v}_h \in X_h. \tag{2.3}$$

As shown in [11], a naive choice of element and triangulation can lead to disastrous results; if $X_h = (P_1)^d$ and a uniform triangulation of the unit square is used, enforcing incompressibility and homogeneous Dirichlet boundary conditions leaves only $\mathbf{u} = \mathbf{0}$ as a possible solution, and thus for nearly-incompressible media, one cannot expect any degree of accuracy. On general meshes, only for $X_h = (P_k)^d$ with $k \geq 4$ in 2D and $k \geq 8$ in 3D optimal accuracy can be expected [28, 34], since in these cases the divergence free subspace of X_h retains optimal approximation properties. However, as discussed in the introduction, on a barycenter refined quasi-uniform mesh, we need only $k \geq 2$ in 2D and $k \geq 3$ in 3D. This is a consequence of the result in [42]. Indeed, let $\tilde{p}_h = -\gamma\mathrm{div}\,\mathbf{u}_h$, $\varepsilon = \gamma^{-1}$. Thanks to the embedding $(\mathrm{div}\,(P_k)^d) \subset P_{k-1}^{disc}$, the elasticity problem (2.3) is equivalent to the penalized finite element Stokes problem

$$2\mu(D(\mathbf{u}_h), D(\mathbf{v}_h)) - (\tilde{p}_h, \mathrm{div}\,\mathbf{v}_h) = (\mathbf{f}, \mathbf{v}_h), \quad \forall\, \mathbf{v}_h \in X_h = (P_k)^d, \tag{2.4}$$

$$(\mathrm{div}\,\mathbf{u}_h, q_h) + \epsilon(\tilde{p}_h, q_h) = 0, \quad \forall\, q_h \in Q_h = P_{k-1}^{disc}. \tag{2.5}$$

Since the resulting finite element pair (X_h, Q_h) is conforming and LBB stable, the standard results, see, e.g., [10], lead to the optimal order convergence of $\mathbf{u}_h, \tilde{p}_h$ to the corresponding solution of the penalized continuous Stokes problem $\mathbf{u}^\varepsilon, p^\varepsilon$:

$$\mu\|\nabla(\mathbf{u}^\varepsilon - \mathbf{u}_h)\| + \|p^\varepsilon - \tilde{p}_h\| \leq ch^k(\|\mathbf{u}^\varepsilon\|_{k+1} + \|p^\varepsilon\|_k) \tag{2.6}$$

with a constant c independent of ε. Lemma 1.1 from [9] yields that for domains with sufficiently regular boundary the norm on the right-hand side of (2.6) is uniformly bounded in ε. Since $\mathbf{u}_\varepsilon$ also solves (2.1) and (2.2) with $\mathbf{g} = \mathbf{0}$, the above discussion implies that for large γ, if $k \geq d$ and a barycenter refined mesh is used, solutions of (2.3) will have optimal accuracy, independent of γ, in the energy norm

$$\|\boldsymbol{\phi}\|_e := \sqrt{\mu\|\boldsymbol{\phi}\|_1^2 + \gamma\|\mathrm{div}\,\boldsymbol{\phi}\|^2}.$$

2.1. Numerical experiment: Convergence rates for Poisson ratio ≈ 0.5. We now demonstrate the effectiveness of the method (2.3) with a test problem used in [18], by testing the method (2.3) on a problem with large γ and known analytical solution using $X_h = (P_2)^2$, a barycenter refined mesh, a uniform mesh, and a mesh created from a Delaunay triangulation. From the above discussion, we expect optimal accuracy when computing with the barycenter refined mesh, and suboptimal accuracy in the other two cases. We find precisely this.

The known solution is given by

$$\mathbf{u}(\mathbf{x}) = \left(-\frac{\gamma + 3\mu}{4\pi\mu(\gamma + 2\mu)} \log \|\mathbf{x} - \mathbf{x}_0\| \mathbf{I} + \frac{\gamma + \mu}{4\pi\mu(\gamma + 2\mu)} \frac{(\mathbf{x} - \mathbf{x}_0)(\mathbf{x} - \mathbf{x}_0)^T}{\|\mathbf{x} - \mathbf{x}_0\|^2} \right) \begin{pmatrix} 1 \\ 0 \end{pmatrix}.$$

We compute on the domain $\Omega = (-1/2, 1/2)^2$, and take $\mathbf{x}_0 =< 1, 0 >^T$, $E = 1$ and $\nu = 0.49999$, which gives the parameters $\mu = 0.3333$ and $\gamma = 1.6667E + 4$, $\mathbf{f} = \mathbf{0}$, and use the known solution's boundary values as Dirichlet boundary data for the computed solutions enforced at every boundary node.

Using successively finer meshes, we compute errors and convergence rates for the method (2.3). The results are given in Table 2.1 for the barycenter refined triangular mesh, and in Table 2.2 for the uniform triangular mesh and the mesh created by a Delaunay triangulation. As expected, in Table 2.1 we see optimal convergence rates for the method (2.3) when the barycenter refined mesh is used. For the uniform mesh and the Delaunay triangulation computations, we observe from Table 2.2 that the convergence rate deteriorates as the mesh width decreases. Moreover, a simple comparison of accuracy versus degrees of freedom between the tables show a dramatic gain in accuracy when a barycenter refined mesh is used.

TABLE 2.1
Convergence of the solution to (2.3) with $X_h = (P_2)^2$ on a barycenter refined uniform mesh of the $(-1/2, 1/2)^2$ square. The convergence rate is optimal.

h	$dim(X_h)$	$\|\mathbf{u}_h - \mathbf{u}_{true}\|_e$	rate
$1/4$	466	9.2464E-3	-
$1/8$	1,914	2.2137E-3	2.06
$1/16$	7,258	5.8160E-4	1.93
$1/32$	29,370	1.5266E-4	1.93
$1/64$	117,106	3.8387E-5	1.99

TABLE 2.2
Convergence of the solution to (2.3) with $X_h = (P_2)^2$ on a uniform mesh of the $(-1/2, 1/2)^2$ square (left), and on Delaunay triangulations (right). Both rates appears sub-optimal.

h	$dim(X_h)$	$\|\mathbf{u}_h - \mathbf{u}_{true}\|_e$	rate	h	$dim(X_h)$	$\|\mathbf{u}_h - \mathbf{u}_{true}\|_e$	rate
$1/2$	50	2.258E-0	-	$\frac{1}{2}$	50	2.258E-0	-
$1/4$	162	4.726E-1	2.26	$1/4$	162	4.726E-1	2.25
$1/8$	578	1.127E-1	2.07	$1/8$	682	3.197E-2	2.07
$1/16$	2,178	2.870E-2	1.97	$1/16$	2,506	4.260E-3	3.09
$1/32$	8,450	7.906E-3	1.86	$1/32$	9,962	8.270E-4	2.38
$1/64$	33,282	2.468E-3	1.68	$1/64$	39,378	1.934E-4	2.11
$1/96$	74,498	1.301E-3	1.58	$1/96$	87,786	8.979E-5	1.91
$1/128$	132,098	8.253E-4	1.58	$1/128$	157,554	5.894E-5	1.44

2.2. Numerical experiment: Mixed boundary conditions. We now numerically test the estimate (2.6) for the case of mixed boundary conditions, where the boundary is divided into pieces, $\partial\Omega = \Gamma_N \cup \Gamma_D$, $\Gamma_N \cap \Gamma_D = \emptyset$, with a Dirichlet condition enforced on Γ_D and the natural boundary condition (described in [1], arising from integration by parts),

$$(-\gamma(\nabla \cdot \mathbf{u}_h) + 2\mu D(\mathbf{u}_h))\,\mathbf{n} = \mathbf{s},$$

is enforced on Γ_N. To our knowledge, the convergence result (2.6) has not been extended to the case of mixed boundary conditions. This is likely due to the proof of (2.6) using a Stokes regularity result, and thus it is not clear how to extend to a boundary condition for Stokes that includes a nonzero divergence term. Still, whether optimal accuracy still holds on barycenter refined meshes, when such boundary conditions are used in linear elasticity is an important question, and thus we consider it numerically.

This numerical experiment uses the same test problem and data as used above in the first numerical experiment, except here we apply Dirichlet boundary conditions to the top, bottom and left-hand sides of the square, and let Γ_N be the right side of the square, $\Gamma_N = \{(x,y) \in \partial\Omega,\ x = 1/2\}$. We compute the function $\mathbf{s}$ from the true solution for $\mathbf{n} = \langle 1, 0\rangle^T$, and use the same barycenter refined meshes from the first experiment. Results are given in Table 2.2, and show that optimal convergence appears to hold, at least for this test example.

TABLE 2.3
Convergence of the solution to (2.3) with $X_h = (P_2)^2$ on a barycenter refined uniform mesh of the $(-1/2, 1/2)^2$ square, with mixed Dirichlet and natural boundary conditions. The convergence rate appears to be optimal.

h	$\|\mathbf{u}_h - \mathbf{u}_{true}\|_e$	rate
$1/4$	7.321E-3	-
$1/8$	1.986E-3	1.88
$1/16$	5.395E-4	1.88
$1/32$	1.460E-4	1.89
$1/64$	3.741E-5	1.97

3. Application to incompressible fluid flow. Consider the classical penalty method for the incompressible Navier-Stokes equations given in the introduction by (1.1),

$$\left\{ \begin{array}{l} \mathbf{u}^\varepsilon_t - \nu\Delta\mathbf{u}^\varepsilon + (\mathbf{u}^\varepsilon \cdot \nabla)\mathbf{u}^\varepsilon + \frac{1}{2}(\operatorname{div}\mathbf{u}^\varepsilon)\mathbf{u}^\varepsilon + \nabla p^\varepsilon = \mathbf{f}, \\ \operatorname{div}\mathbf{u}^\varepsilon + \varepsilon p^\varepsilon = 0, \quad \mathbf{u}^\varepsilon|_{t=0} = \mathbf{u}^0. \end{array} \right. \tag{3.1}$$

There are several ways to approach the equations numerically. One is to apply a finite element method directly to (3.1): Given an LBB stable velocity-pressure pair

$$(X_h, Q_h) \subset ((H^1_0(\Omega))^d, L^2_0(\Omega)),$$

on a regular triangular (tetrahedral) mesh of a polygonal (polyhedral) domain $\Omega \subset \mathbb{R}^d$, find $(\mathbf{u}^\varepsilon_h, p^\varepsilon_h) \in (X_h, Q_h) \times (0, T]$ satisfying

$$\left\{ \begin{array}{l} ((\mathbf{u}^\varepsilon_h)_t, \mathbf{v}_h) + b(\mathbf{u}^\varepsilon_h, \mathbf{u}^\varepsilon_h, \mathbf{v}_h) - (p^\varepsilon_h, \operatorname{div}\mathbf{v}_h) + \nu(\nabla\mathbf{u}^\varepsilon_h, \nabla\mathbf{v}_h) = (\mathbf{f}, \mathbf{v}_h), \\ (\operatorname{div}\mathbf{u}^\varepsilon_h, q_h) + \varepsilon(p^\varepsilon_h, q_h) = 0, \end{array} \right. \tag{3.2}$$

for all $\mathbf{v}_h \in X_h, q_h \in Q_h$ with

$$b(\mathbf{u}, \mathbf{w}, \mathbf{v}) := (\mathbf{u} \cdot \nabla\mathbf{w}, \mathbf{v}) + \frac{1}{2}((\operatorname{div}\mathbf{u})\mathbf{w}, \mathbf{v}), \ \text{ and } \ \mathbf{u}^\varepsilon_h|_{t=0} = I_h(\mathbf{u}_0),$$

where $I_h(\mathbf{u}_0)$ is an appropriate interpolant. The finite element formulation (3.2) is convenient for error analysis; in particular, convergence to the solution of (3.1), uniformly in ε, can be proved, see [21] for analysis in 2D. However, (3.2) may be impractical from the computational point of view. Indeed, eliminating the pressure variable from (3.2) leads to the system of algebraic equations which involves the matrix of the form $\varepsilon^{-1}B^TM^{-1}B$, where B is the finite element divergence matrix and M is the mass matrix for Q_h. Except for a few special cases, M^{-1} is *not* a sparse matrix. Thus solving the system becomes too expensive even for a moderate number of unknowns. One may alter the problem and consider a sparse (e.g., diagonal) approximation of M^{-1}, hence deviating from the finite element formulation (3.2). This would reduce the cost significantly, however, in terms of matrix fill-in, the approach still remains inferior to the direct discretization of (1.2): Given a velocity finite element space $X_h \subset (H_0^1(\Omega))^d$, find $\mathbf{u}_h^\varepsilon \in X_h \times (0,T]$ satisfying

$$((\mathbf{u}_h^\varepsilon)_t, v_h) + b(\mathbf{u}_h^\varepsilon, \mathbf{u}_h^\varepsilon, \mathbf{v}_h) + \varepsilon^{-1}(\operatorname{div}\mathbf{u}_h^\varepsilon, \operatorname{div}\mathbf{v}_h) + \nu(\nabla\mathbf{u}_h^\varepsilon, \nabla\mathbf{v}_h) = (\mathbf{f}, \mathbf{v}_h), \tag{3.3}$$

for all $\mathbf{v}_h \in X_h, q_h \in Q_h$ and $\mathbf{u}_h^\varepsilon|_{t=0} = I_h(\mathbf{u}_0)$. Below we compare the fill-in properties and solver timings for (3.2) vs. (3.3). Concerning the accuracy of (3.3), we note that for arbitrarily chosen finite element spaces, the method may exhibit the loss of accuracy for small values of ε due to the same phenomena as locking in linear elasticity. To avoid locking we assume:
(A1): the mesh is created as a barycenter refinement of a regular triangulation (tetrahedralization),
(A2): the velocity space is chosen to be piecewise polynomials of degree k, with k at least as large as the space dimension: $X_h = (P_k)^d$, with $k \geq d$.

The following result is the key to an obtaining optimal ε-uniform error estimate for the penalty finite element method (3.3). It is the simple consequence of the LBB stability of the Scott-Vogelius element, but to our knowledge has not yet been written down in the literature. For all estimates below, we assume the family of meshes satisfies minimum angle condition, and denote by h the maximum element diameter for a fixed mesh.

LEMMA 3.1. *Assume* (A1), (A2), *and* Ω *is convex. For any* $\mathbf{v} \in \mathbf{H}^{k+1} \cap \mathbf{H}_0^1$, $k \geq d$, *there exists a finite element function* $\mathbf{v}_h \in X_h$ *such that*

$$\|\mathbf{v} - \mathbf{v}_h\| + h\|\nabla(\mathbf{v} - \mathbf{v}_h)\| \leq c\, h^{k+1}\|\mathbf{v}\|_{k+1}, \tag{3.4}$$

$$\|\operatorname{div}(\mathbf{v} - \mathbf{v}_h)\| \leq c\, h^{k}\|\operatorname{div}\mathbf{v}\|_{k}. \tag{3.5}$$

Proof. Complement X_h with the pressure space Q_h of P_{k-1}^{disc} elements. Under the assumptions of the lemma (X_h, Q_h), form the LBB stable Stokes element and $\operatorname{div} X_h \subset Q_h$. Consider $\mathbf{v}_h$ as the velocity solution to the discrete Stokes type problem

$$(\nabla\mathbf{v}_h, \nabla\boldsymbol{\psi}_h) - (q_h, \operatorname{div}\boldsymbol{\psi}_h) + (\operatorname{div}\mathbf{v}_h, \xi_h) = (\nabla\mathbf{v}, \nabla\boldsymbol{\psi}_h) + (\operatorname{div}\mathbf{v}, \xi_h), \tag{3.6}$$

$\forall\, \boldsymbol{\psi}_h \in X_h, \xi_h \in Q_h$. Thanks to the LBB stability of (X_h, Q_h) and regularity assumption on Ω, the standard error estimate for the finite element solution to the Stokes problem yields the estimate (3.4). Moreover, the inclusion $\operatorname{div} X_h \subset Q_h$ and (3.6) imply $\operatorname{div}\mathbf{v}_h = P_Q \operatorname{div}\mathbf{v}$, where P_Q is the L^2 orthogonal projector on Q_h. Therefore,

$$\|\operatorname{div}(\mathbf{v} - \mathbf{v}_h)\| = \|\operatorname{div}\mathbf{v} - P_Q\operatorname{div}\mathbf{v}\| = \inf_{q_h \in Q_h}\|\operatorname{div}\mathbf{v} - q_h\| \leq c\, h^{k}\|\operatorname{div}\mathbf{v}\|_{k}. \qquad \square$$

Lemma 3.1 shows that the divergence free subspace of X_h is rich enough to provide the optimal approximation properties in the divergence free subspace. This means that *no* locking occurs. For P1 nonconforming elements the result stated in the lemma appears with $k = 1$ in [31] as inequalities (3.11) and (3.12) (page 269) and is the only instance where specific properties of nonconforming P1 elements were used in error analysis. Thus, the analysis of that paper may be applied to conforming elements satisfying assumptions (A1) and (A2), with the simplification that no inter-element non-consistency terms occur. Repeating arguments of [31] shows the following result for the proposed scheme.

THEOREM 3.2. *Let ε be sufficiently small, $\varepsilon < c_\Omega$, where the constant c_Ω depends only on the domain Ω, and the data $\mathbf{u}_0$ and $\mathbf{f}$ is sufficiently small to guarantee that the solution of* (1.2) *is unique (in $3D$). Then for the solutions to* (1.2) *and* (3.3) *it holds*

$$\|\mathbf{u}^\varepsilon(t) - \mathbf{u}_h^\varepsilon(t)\| \le C\,h^2, \quad \|\mathrm{div}\,(\mathbf{u}^\varepsilon(t) - \mathbf{u}_h^\varepsilon(t))\| \le C\,(h + t^{-1}h^2) \quad \forall\, t \in [0,T]\,, \tag{3.7}$$

with a constant C independent of ε, but dependent on norms of $\mathbf{u}_0$ and $\mathbf{f}$.

Recover finite element pressure through $p_h^\varepsilon := -\varepsilon^{-1}\mathrm{div}\,\mathbf{u}_h^\varepsilon$. The bound (3.7) can be combined with the result of Shen in (1.3) to estimate the convergence of the finite element penalized solution to the true Navier-Stokes solution:

$$\|\mathbf{u}(t) - \mathbf{u}_h^\varepsilon(t)\| \le C\,(h^2 + t^{-\frac{1}{2}}\varepsilon), \quad \int_0^t s^2\|p(s) - p_h^\varepsilon(s)\|\,\mathrm{d}t \le C\,(h + \varepsilon),\ \forall\, t \in [0,T]. \tag{3.8}$$

Clearly, for P^k ($k \ge d$) conforming elements the theoretically justified estimates (3.7), (3.8) are suboptimal in terms of convergence order. The optimal estimates would likely read

$$\|\mathbf{u}^\varepsilon(t) - \mathbf{u}_h^\varepsilon(t)\| \le C\,h^{k+1} \text{ and } \|\mathbf{u}(t) - \mathbf{u}_h^\varepsilon(t)\| \le C\,(h^{k+1} + t^{-\frac{1}{2}}\varepsilon),\ \forall\, t \in [0,T]. \tag{3.9}$$

There are technical difficulties to generalize the analysis for the case $k > 1$ in the optimal way: standard approximation properties of finite elements would involve higher order norms of $\mathbf{u}^\varepsilon$ in the definition of the constant C in the right-hand sides of (3.9). To show that C does not depend on ε one needs ε-independent bounds of the higher order norms of $\mathbf{u}^\varepsilon$ by the given data. We are not aware of such bounds available in the literature. However, in section 3.1, we show results of numerical experiments which suggest that (3.9) holds.

We now consider five test problems to demonstrate the effectiveness of the proposed method. The first test is a numerical verification of the hypothesized convergence rates for (3.3) on a model problem. Next, we compare accuracy and complexity of the method (3.3) with that of (3.2) with both Scott-Vogelius and Taylor-Hood elements. The third experiment is for the 2d benchmark problem of flow over a step, where we compare the solution of (3.3) with that of (3.2), again with both Scott-Vogelius and Taylor-Hood elements. The final two experiments are for the 3D driven cavity and 3D channel flow over a forward-backward step. For both of these larger tests, we show that the method (3.3) remains accurate and efficient. All computations were performed using the second author's finite element codes written in Matlab, and all timings were made on a Macbook Pro with 2x 2.66 GHz Intel Quad-Core 2 Xeon with 12GB 10 MHz DDR3 memory. All linear solves were performed directly with sparse banded Gaussian elimination (Matlab's "backslash").

3.1. Numerical experiment: convergence rates. It is shown above that for conforming elements, provided (A1) and (A2) hold, the estimate (3.7) holds, which leads to the hypothesized error estimate

$$\|\mathbf{u}(t) - \mathbf{u}_h^\varepsilon(t)\| \le C\,(h^{k+1} + t^{-\frac{1}{2}}\varepsilon),\ \forall\, t \in [0,T]\,. \tag{3.10}$$

As discussed above, proving this estimate appears to require significant technical effort. We now provide numerical evidence that suggests a discrete analog of it to hold. With a Crank-Nicolson temporal discretization and fixed endtime T, the discrete analog becomes

$$\|\mathbf{u}(T) - \mathbf{u}_h^\varepsilon(T)\| \le C\,(h^{k+1} + \varepsilon + \Delta t^2), \tag{3.11}$$

where C depends on the data, including $T = O(1)$. We note that, for a fixed T, mesh, and time step, the $O(\epsilon)$ convergence has been shown numerically in [12].

ETNA
Kent State University
http://etna.math.kent.edu

We determine approximations of the exact solutions,

$$\mathbf{u}(x,y,t) = (1+0.01t)\begin{pmatrix} 2x^2(x-1)^2y(2y-1)(y-1) \\ -2x(x-1)(2x-1)y^2(y-1)^2 \end{pmatrix}, \quad p = y, \tag{3.12}$$

of the 2D model problem studied in [25]: A plot of the true solution in given in Figure 3.1. Using $\nu = 1$, $T = 0.1$, $\mathbf{f}$ is calculated from the NSE and solution, and using the domain $\Omega = (0,1)^2$, we solve (3.3) with $X_h = (P_2)^2$ (i.e., $k = 2$). The meshes used are barycenter refined meshes; also shown in Figure 3.1 is the mesh used for $h = 1/8$. Note that both assumptions (A1) and (A2) are satisfied.

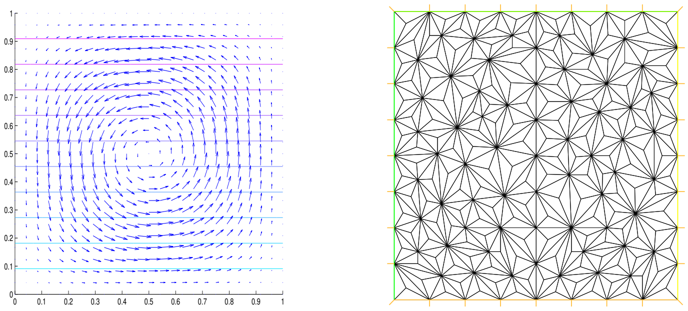

FIG. 3.1. *Shown above is: (left) the velocity vector field of true solution for convergence rate numerical experiment , and (right) the $h = 1/8$ barycenter refined mesh.*

We compute the error for solutions resulting from successively refined meshes, time steps, and ϵ. We successively refine the meshes, and tie the time step and ϵ to this refinement so that the hypothesized error is $O(h^{k+1})$ (i.e., with $k = 2$, if h gets cut in half, ϵ gets cut in eighth, and Δt gets cut in third). Results are shown in Table 3.1, and the hypothesized rate is observed.

TABLE 3.1
Errors and rates for varying h, ϵ, and Δt. Optimal convergence is observed.

h	Δt	$dim(X_h)$	ϵ	$\lVert\mathbf{u}(T) - \mathbf{u}_h^{\epsilon}(T)\rVert$	rate
$1/4$	T	466	$1/100$	1.480E-3	
$1/8$	$T/3$	1,914	$1/800$	1.375E-4	3.42
$1/16$	$T/9$	12,604	$1/6,400$	1.651E-5	3.06
$1/32$	$T/27$	29,370	$1/51,200$	2.029E-6	3.02
$1/64$	$T/81$	117,106	$1/409,600$	2.533E-7	3.00

3.2. Numerical experiment: comparison of methods. We discuss two methods for eliminating the pressure: 'first penalize, discretize then eliminate pressure' and 'first penalize, eliminate then discretize'. They lead to (3.2) and (3.3), respectively. The method (3.3) solves directly for velocity only, and the system resulting from (3.2) can be manipulated to solve for only the velocity. As discussed above, for this second method to be efficient, a sparse approximation to $B^T M^{-1} B$ must be made, where B is the matrix arising from the inner product $(\operatorname{div} \mathbf{u}_h, q_h)$ and M is the pressure mass matrix arising from (p_h, q_h). A common choice is to replace $B^T M^{-1} B$ by $B^T(\operatorname{diag}(M))^{-1}B$, and we use this "approximation" in this experiment.

We consider again the NSE spinning eddy problem (3.12), but for simplicity now in the steady case. We compute (3.3) with $X_h = (P_2)^2$, and (3.2) with both $((P_2)^2, P_1^{disc})$ Scott-Vogelius elements and $((P_2)^2, P_1)$ Taylor-Hood elements, using $\nu = 0.01$, and the $h = 1/32$ barycenter refined mesh. As was noted already in Section 2, due to the embedding $(\mathrm{div}\,(P_k)^d) \subset P_{k-1}^{disc}$, the Scott-Vogelius element is the special element when both approaches, i.e., discretizing (3.3) or first discretizing (3.2) and then eliminating pressure, are equivalent and lead to the same system of algebraic equations (in this case $B^T M^{-1} B$ appears to be sparse). This is, however, *not* the case for the majority of elements used in practice. Further, in the tables, "SV for (3.2)" stands for the following simplification: For Scott-Vogelius element (similar to Taylor-Hood) the matrix $B^T M^{-1} B$ is replaced by $B^T (diag(M))^{-1} B$. We will see that this alteration results in an approach with properties similar to (3.3), although slightly less efficiently.

Errors and solve times for this experiment are given in Table 3.2. We find that the proposed method (3.3) and the method (3.2) with Scott-Vogelius elements gave solutions that had comparable accuracy, but the method (3.2) with Taylor-Hood elements was significantly worse. For solve times, the method (3.3) was slightly faster than (3.2) with Scott-Vogelius elements, but both of these were much faster than (3.2) with Taylor-Hood elements. Further investigation of the sparsity structures revealed that the resulting matrix used in Taylor-Hood had significantly more nonzeros, which led to its significantly worse solve times (see Table 3.2 and Figure 3.2). Although the B matrix for Taylor-Hood is smaller than for Scott-Vogelius (due to continuous versus discontinuous pressure space), its density causes $B^T(\mathrm{diag}(M))^{-1}B$ to be a much denser matrix than in the Scott-Vogelius case.

TABLE 3.2
Errors, solve times, and number of system matrix nonzeros for the different methods for computing the 2D spinning eddy on the $h = 1/32$ barycenter refined mesh.

Method	$\|\mathbf{u} - \mathbf{u}_h^\varepsilon\|$	average solve time	nonzeros in system matrix
(3.3)	1.722E-4	0.461 sec.	667,936
(3.2), SV	1.683E-4	0.475 sec.	670,671
(3.2), TH	1.098E-3	39.61 sec.	4,570588

3.3. Numerical experiment: 2D channel flow over a forward-backward step. For the next test, we consider the benchmark problem of 2D flow over a forward and backward facing step. This problem is time dependent, and we choose the linearly extrapolated Crank-Nicolson (CNLE) method of Baker [3] for the temporal discretization. This is a natural choice due to its unconditional stability with respect to time step size, and second order accuracy.

This problem has been studied in [20, 24, 32], and consists of a 40×10 rectangular channel with a 1×1 step on the bottom of the channel, 5 units in. The inflow boundary is set as a Dirichlet parabolic condition,

$$\mathbf{u}(0, y, t) = [y(10 - y)/25, 0]^T,$$

the top, sides and step have no-slip boundary conditions, and at the outflow boundary the 'do-nothing' condition is enforced. The viscosity is chosen to be $\nu = \frac{1}{600}$, and the forcing is taken to be zero, $\mathbf{f} = \mathbf{0}$. The simulation is run from an initial condition of fully parabolic flow throughout the channel, with the step being inserted at time $t = 0$, and then the problem is run to $T = 40$. The correct physical behavior is for eddies to form behind the step, then detach and move down the channel, with new eddies forming.

We compute solutions to this problem using (3.3) with $X_h = (P_2)^2$, and with (3.2) by eliminating pressure and replacing $B^T M^{-1} B$ with $B^T(\mathrm{diag}(M)^{-1})B$ for both $((P_2)^2, P_1^{disc})$

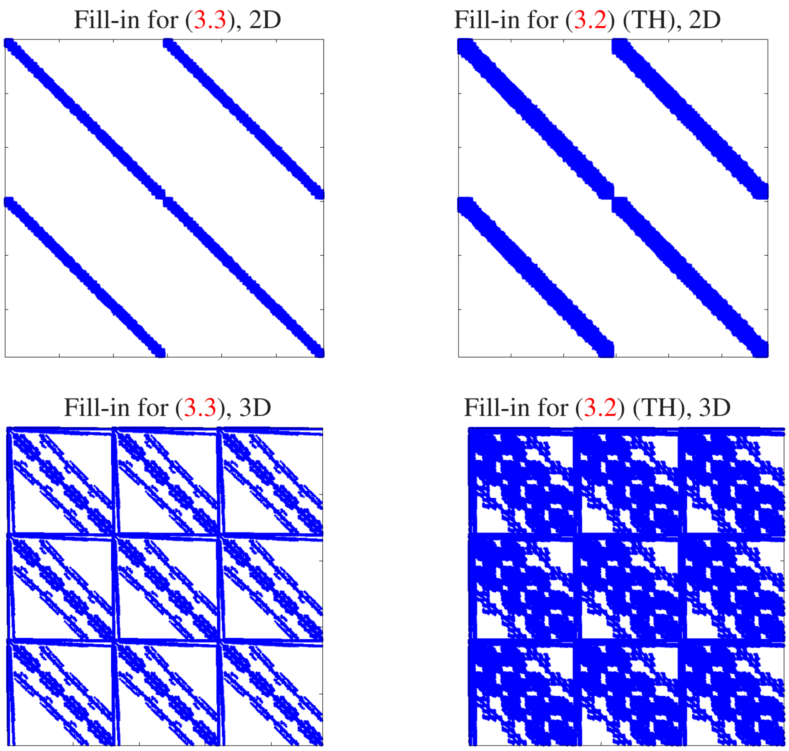

FIG. 3.2. *Fill-in patterns for the system matrices arising from (3.3) (left), and (3.2) with Taylor-Hood elements after eliminating pressure (right). Top pictures: the 2D test problem of Section 3.1.2 with $h = \frac{1}{32}$. Bottom pictures: The 3D cavity problem, $h = \frac{1}{4}$.*

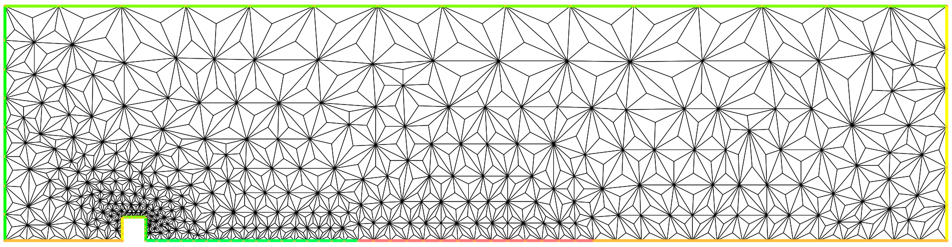

FIG. 3.3. *The barycenter refined mesh used for the 2D channel flow over a step experiment.*

Scott-Vogelius elements and $((P_2)^2, P_1)$ Taylor-Hood elements. In all schemes we choose $\epsilon = 10^{-4}$, time step $\Delta t = 0.01$, and use the mesh in Figure 3.3 which provides 7,414 velocity degrees of freedom for $(P_2)^2$ velocities and 5,418 degrees of freedom for the P_1^{disc} discontinuous pressure space, and 915 degrees of freedom for the P_1 continuous pressure space.

Average solve times and number of nonzeros in the system matrices are given in Table 3.3. We see that the method (3.3) is faster than the methods of (3.2): about 20% faster than

(3.2) with Scott-Vogelius elements and 10 times faster than with Taylor-Hood elements.

TABLE 3.3
Solve times for the different methods for computing 2D flow over a step.

Method	average solve time (4,000 solves)	nonzeros in system matrix
(3.3)	0.081 sec.	166,588
(3.2), SV	0.115 sec.	167,224
(3.2), TH	1.1041 sec.	1,089,882

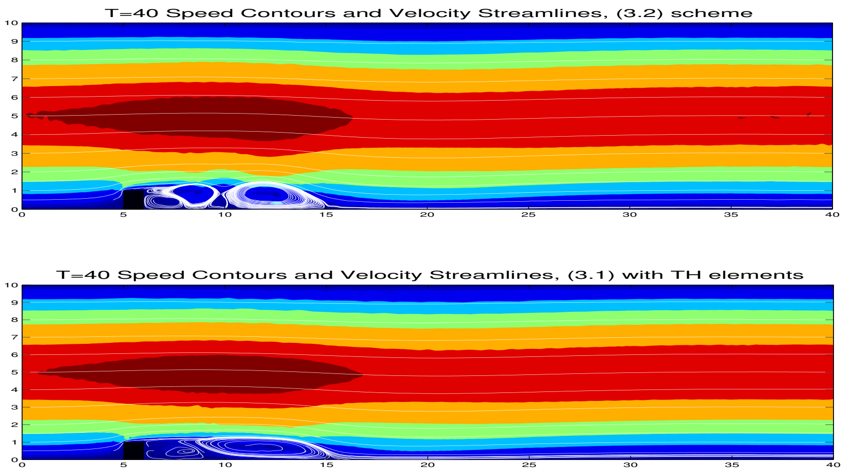

FIG. 3.4. *Shown above are the speed contours and velocity streamlines for the solutions to the 2D step benchmark problem at T=40: (TOP) the* (3.3) *solution, and (BOTTOM) the* (3.2) *solution with Taylor-Hood elements.*

Plots of solutions at $T = 40$ are shown in Figure 3.4 as velocity streamlines over speed contours. The method (3.3) and (3.2) with SV elements both give good solutions that are visually indistinguishable (and so only a plot of (3.3) is shown), although they are slightly different:

$$\|\mathbf{u}_{(3.2),SV} - \mathbf{u}_{(3.3)}\| = 2.722E - 4 \quad \text{for } T = 40.$$

The solution from (3.2) with TH elements, on the other hand, is visibly less resolved. The likely reason is its poor mass conservation compared to the other solutions: at $T = 40$,

$$\begin{aligned} \|\text{div}\, \mathbf{u}_{(3.3)}\| &= 5.296E - 5 \\ \|\text{div}\, \mathbf{u}_{(3.2),SV}\| &= 2.839E - 5 \\ \|\text{div}\, \mathbf{u}_{(3.2),TH}\| &= 1.210E - 0 \end{aligned}$$

3.4. Numerical experiment: 3D driven cavity benchmark problem. This numerical test is for the 3D driven cavity problem at $Re = 100$, 400, and 1,000. This problem is well studied [30, 33, 41], and consists of 3D flow in the unit box where the sides and bottom have prescribed no-slip boundary conditions and the top (moving lid) is given the Dirichlet condition $\mathbf{u} = [1, 0, 0]^T$. There is no forcing with this problem: $\mathbf{f} = \mathbf{0}$, and kinematic viscosities are taken to be $\nu = Re^{-1}$. The solution is known to be steady for each of these Reynolds numbers.

We computed on a barycenter refinement of a quasi-uniform tetrahedral mesh using $X_h = (P_3)^3$ velocity elements, which gives 185,115 velocity degrees of freedom. We compute only with (3.3) for this experiment, and note that the $((P_3)^2, P_2^{disc})$ SV element implementation has 306,753 total dof. Again we take $\varepsilon = 10^{-4}$, and use Newton's method (without relaxation) to solve the nonlinear problem. The linear solves averaged 20.3 seconds! For a problem of this size, such a solve time is competitive with most preconditioned iterative methods applied to the mixed method's saddle point systems, although the direct solve is certainly more robust.

Plots of the solutions are shown in Figure 3.5 as midplane velocities. The results agree well with simulation data given in [30, 41], and thus we see again that the proposed method (3.3) is accurate as well as efficient.

As expected, mass conservation by each of the solutions was also very good:

$$\begin{array}{rrcl} \text{Re} = & 100 & : & \|\text{div}\,\mathbf{u}_h\| = 1.917E-5, \\ \text{Re} = & 400 & : & \|\text{div}\,\mathbf{u}_h\| = 7.764E-6, \\ \text{Re} = & 1,000 & : & \|\text{div}\,\mathbf{u}_h\| = 4.395E-6. \end{array}$$

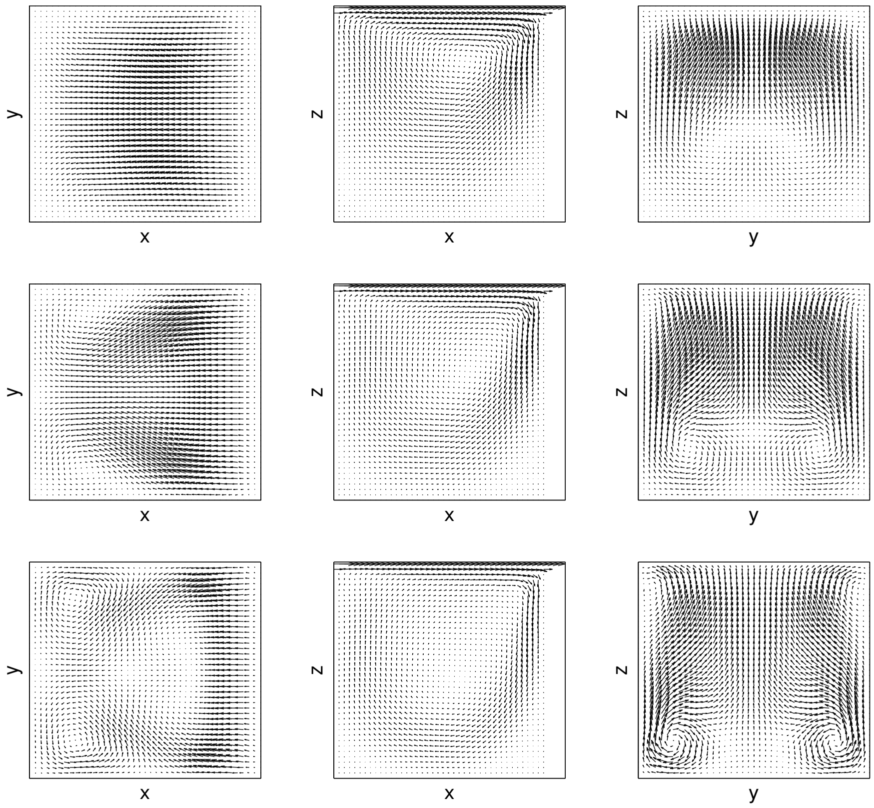

FIG. 3.5. *Shown above are the midplane velocity vector fields for the computed solution with TOP ROW: Re=100, MIDDLE ROW: Re=400, BOTTOM ROW: Re=1,000.*

3.5. Numerical experiment: 3D flow over a forward-backward facing step. The final numerical experiment is for 3D channel flow over a forward and backward facing step.

This problem was computed by V. John and A. Liakos in [23], and consists of a $10 \times 40 \times 10$ rectangular channel with a $10 \times 1 \times 1$ block step on the bottom of the channel, 5 units in. As in [23], we take a constant inflow $u = [0, 1, 0]$, no slip boundary conditions on the channel walls, a zero traction outflow condition, and use viscosity $\nu = 1/20$. Computations were performed on a barycenter refined tetrahedral mesh using (3.3) with $\varepsilon = 10^{-4}$, $X_h = (P_3)^3$ with 376,500 velocity dof (the corresponding SV problem would have 602,060 total dof). It took 6 iterations to converge for the Newton method, and the average time per linear solve was 61.4 seconds.

The results obtained are in agreement with those found in [23]. Plots of the solution are shown in Figure 3.6, as a sliceplane of streamlines and speed contours, and zoomed in, and a plot of the reattachment line.

4. Conclusions and Future Directions. By using a barycenter refined triangular / tetrahedral mesh and $k \geq d$, accurate approximations can be found for the linear elasticity problem in pure displacement formulation with Poisson ratio ≈ 0.5, and incompressible flow problems can be accurately and efficiently computed with 'velocity-only' linear solves. The results extend to $k < d$ in some situations, provided that more elaborate macro-element structures are used, with the key requirement being that the SV element pair is LBB stable.

Of particular interest for future work is extending the applicability of the developed incompressible flow methods to larger problems. We have shown numerical examples where these methods are accurate, very efficient, provide excellent mass conservation, and are highly competitive with state of the art preconditioned iterative methods (e.g., [4, 5, 6]) applied to the associated saddle point problems. The excellent mass conservation and compliance with robust of-the-shelf direct solvers (such as Matlab's "backslash") makes the properly designed penalty method an attractive alternative to other pressure decoupling approaches such as projection and artificial compressibility methods. However, the problem size where the methods are currently applicable appears limited to about 1 million (or so) dof in 3D, and thus finding ways around this limitation would be also of interest to many CFD practicioners. For example, different matrix structuring or factorizations could lead to easier direct solves. The iterated penalty method [43] could also be used, which would lower the effective artificial compressibility parameter and allow for iterative solvers, but with the cost of tripling (or more) the total number of linear solves needing done.

REFERENCES

[1] D. ARNOLD AND R. FALK, *Well-posedness of the fundamental boundary value problems for constrained anisotropic elastic materials*, Arch. Rational Mech. Anal., 98 (1987), pp. 143–167.
[2] D. N. ARNOLD AND J. QIN, *Quadratic velocity/linear pressure Stokes elements*, in Advances in Computer Methods for Partial Differential Equations VII, R. Vichnevetsky, D. Knight, and G. Richter, eds., IMACS, 1992, pp. 28–34.
[3] G. BAKER, *Galerkin approximations for the Navier-Stokes equations*, Technical Report, Department of Mathematics, Harvard University, (1976).
[4] M. BENZI, G. GOLUB, AND J. LIESEN, *Numerical solution of saddle point problems*, Acta Numerica, 14 (2005), pp. 1–137.
[5] M. BENZI, M. OLSHANSKII, AND Z. WANG, *Modified augmented Lagrangian preconditioners for the incompressible Navier-Stokes equations*, Internat. J. Numer. Methods Fluids, 66 (2011), pp. 486–508.
[6] M. BENZI AND M. A. OLSHANSKII, *An augmented Lagrangian-based approach to the Oseen problem*, SIAM J. Sci. Comput., 28 (2006), pp. 2095–2113.
[7] S. BÖRM AND S. LE BORNE, *H-LU factorization in preconditioners for augmented Lagrangian and grad-div stabilized saddle point systems*, Internat. J. Numer. Methods Fluids, DOI: 10.1002/fld.2495 (2011).
[8] A. BOWERS, B. COUSINS, A. LINKE, AND L. REBHOLZ, *New connections for finite element formulations of the Navier-Stokes equations*, J. Comput. Phys., 229 (2010), pp. 9020–9025.
[9] B. BREFORT, J. GHIDAGLIA, AND R. TEMAM, *Attractors for the penalized Navier-Stokes equations*, SIAM J. Math. Anal., 19 (1988), pp. 1–21.

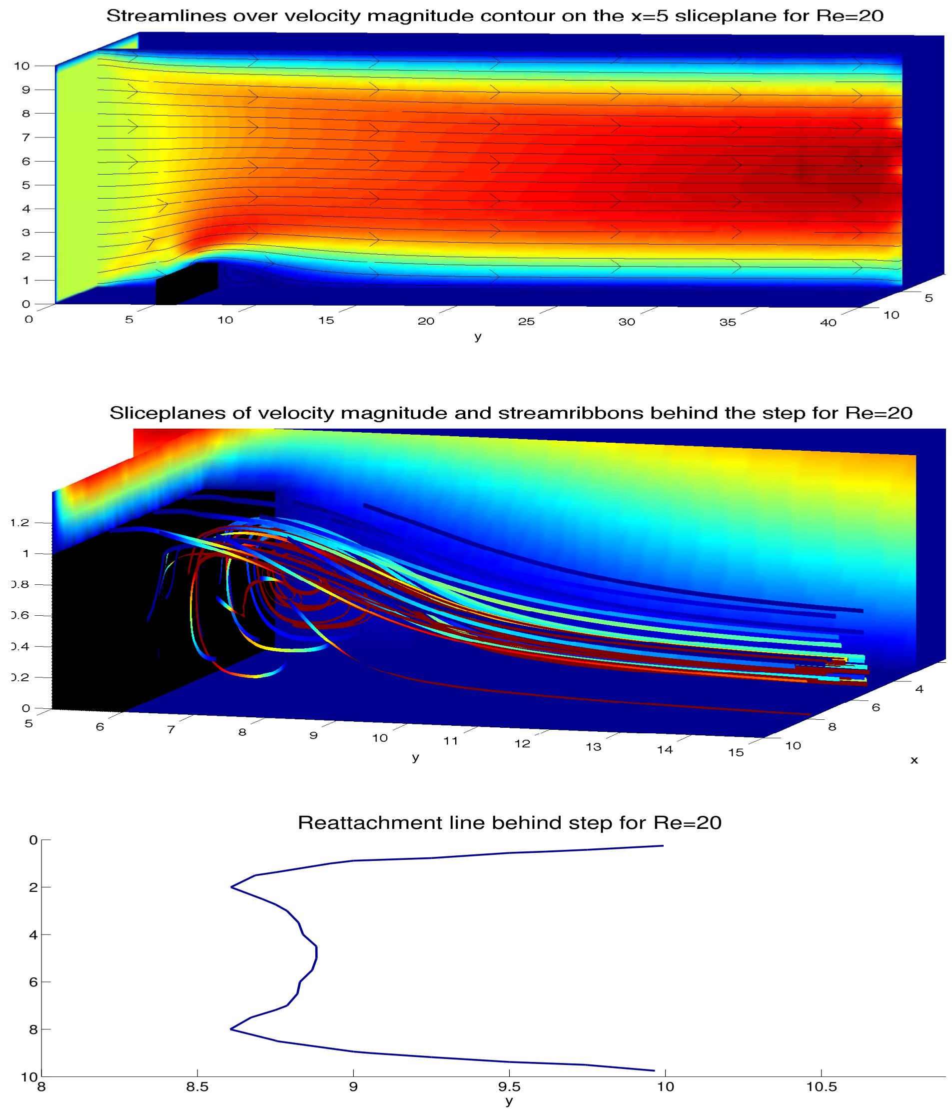

FIG. 3.6. *Shown above are the $x = 5$ sliceplane of speed contours and velocity streamlines (TOP), a 'zoomed-in' picture behind the step with velocity streamribbons (MIDDLE), and the reattachment line behind the step (BOTTOM).*

[10] S. BRENNER, *Multigrid methods for parameter dependent problems*, RAIRO, Model. Math. Anal. Numer., 30 (1996), pp. 265–297.

[11] S. BRENNER AND L. SCOTT, *The Mathematical Theory of Finite Element Methods*, Springer, New York, 1994.

[12] M. CASE, V. ERVIN, A. LINKE, AND L. REBHOLZ, *A connection between Scott-Vogelius elements and grad-div stabilized taylor-hood fe approximations of the navier-stokes equations*, SIAM J. Numer. Anal., 49 (2011), pp. 1461–1481.

[13] A. J. CHORIN, *A numerical method for solving incompressible viscous flow problems*, J. Comput. Phys., 2 (1967), pp. 12–26.

[14] ———, *Numerical solution for the Navier-Stokes equations*, Math. Comp., 22 (1968), pp. 745–762.

[15] C. DOHRMANN AND O. WIDLUND, *An overlapping Schwarz algorithm for almost incompressible elasticity*, SIAM J. Numer. Anal, 47 (2009), pp. 2897–2923.

[16] E. D'YAKONOV, *Regular perturbations of nonstationary problems of mathematical physics related to linear constraints: I*, Diff. Equat., 37 (2001), pp. 58–69.

[17] L. FRANCA AND R. STENBERG, *Error analysis of some Galerkin least squares methods for the elasticity equations*, SIAM J. Numer. Anal., 28 (1991), pp. 1680–1697.

[18] G. GATICA, A. MARQUEZ, AND S. MEDDAHI, *A new dual-mixed finite element method for the plane linear elasticity problem with pure traction boundary conditions*, Comput. Methods Appl. Mech. Engrg., 197 (2008), pp. 1115–1130.

[19] V. GIRAULT AND P.-A. RAVIART, *Finite Element Methods for Navier-Stokes equations : Theory and Algorithms*, Springer-New York, 1986.

[20] M. GUNZBURGER, *Finite Element Methods for Viscous Incompressible Flow: A Guide to Theory, Practice, and Algorithms*, Academic Press, Boston, 1989.

[21] Y. HE, *Optimal error estimate of the penalty finite element method for the time-dependent Navier-Stokes equations*, Math. Comp., 74 (2005), pp. 1201–1216.

[22] J. HEINRICH AND V. VIONNET, *The penalty method for the Navier-Stokes equations*, Arch. Comput. Methods Eng., 2 (1995), pp. 51–65.

[23] V. JOHN, *Slip with friction and penetration with resistance boundary conditions for the Navier-Stokes equations - numerical tests and aspects of the implementation*, J. Comput. Appl. Math., 147 (2002), pp. 287–300.

[24] V. JOHN AND A. LIAKOS, *Time dependent flow across a step: the slip with friction boundary condition*, Internat. J. Numer. Methods Fluids, 50 (2006), pp. 713 – 731.

[25] S. KAYA AND B. RIVIERE, *A discontinuous subgrid eddy viscosity method for the time-dependent Navier-Stokes equations*, SIAM J. Numer. Anal., 43 (2005), pp. 1572–1595.

[26] W. LAYTON, *An Introduction to the Numerical Analysis of Viscous Incompressible Flows*, SIAM, Philadelphia, 2008.

[27] Y. LI AND K. LI, *Penalty finite element method for Stokes problem with nonlinear slip boundary conditions*, Appl. Math. Comput., 204 (2008), pp. 216–226.

[28] A. LINKE, *Divergence-free mixed finite elements for the incompressible Navier-Stokes Equation*, PhD thesis, University of Erlangen, 2008.

[29] ———, *Collision in a cross-shaped domain — A steady 2d Navier-Stokes example demonstrating the importance of mass conservation in CFD*, Comp. Meth. Appl. Mech. Eng., 198 (2009), pp. 3278–3286.

[30] D. LO, K. MURUGESAN, AND D. YOUNG, *Numerical solution of three-dimensional velocity-vorticity Navier-Stokes equations by finite difference method*, Internat. J. Numer. Methods Fluids, 47 (2005), pp. 1469–1487.

[31] X. LU AND P. LIN, *Error estimate of the P1 nonconforming finite element method for the penalized unsteady Navier-Stokes equations*, Numer. Math., 115 (2010), pp. 261–287.

[32] C. MANICA, M. NEDA, M. OLSHANSKII, AND L. REBHOLZ, *Enabling accuracy of Navier-Stokes-alpha through deconvolution and enhanced stability*, ESAIM: Mathematical Modelling and Numerical Analysis, 45 (2011), pp. 277–308.

[33] M. OLSHANSKII AND L. REBHOLZ, *Velocity-Vorticity-Helicity formulation and a solver for the Navier-Stokes equations*, J. Comput. Phys., 229 (2010), pp. 4291–4303.

[34] J. QIN, *On the convergence of some low order mixed finite elements for incompressible fluids*, PhD thesis, Department of Mathematics, Pennsylvania State University, 1994.

[35] J. SCHÖBERL, *Multigrid methods for a parameter dependent problem in primal variables*, Numer. Math., 84 (1999), pp. 97–119.

[36] J. SHEN, *On error estimates of the penalty method for unsteady Navier-Stokes equations*, SIAM J. Numer. Anal., 32 (1995), pp. 386–403.

[37] R. STENBERG, *Analysis of mixed finite elements methods for the Stokes problem: A unified approach*, Math. Comp., 42 (1984), pp. 9–23.

[38] R. TEMAM, *Sur lapproximation des solutions des equations de Navier-Stokes*, C.R. Acad. Sci. Paris, Series A, 262 (1966), pp. 219–221.

[39] ———, *Une methode dapproximation des solutions des equations de Navier-Stokes*, Bull Soc. Math. France, 98 (1968), pp. 115–152.

[40] ———, *Navier-Stokes Equations, Theory and Numerical Analysis*, vol. 2, North-Holland Publishing Company, 1979.

[41] K. WONG AND A. BAKER, *A 3d incompressible Navier-Stokes velocity-vorticity weak form finite element algorithm*, Internat. J. Numer. Methods Fluids, 38 (2002), pp. 99–123.

[42] S. ZHANG, *A new family of stable mixed finite elements for the 3d Stokes equations*, Math. Comp., 74 (2005), pp. 543–554.

[43] ———, *On the P1 Powell-Sabin divergence-free finite element for the Stokes equations*, J. Comput. Math., 26 (2008), pp. 456–470.

[44] ———, *Divergence-free finite elements on tetrahedral grids for* $k \geq 6$, Math. Comp., 80 (2011), pp. 669–695.
[45] ———, *Quadratic divergence-free finite elements on Powell-Sabin tetrahedral grids*, Calcolo, 48 (2011), pp. 211–244.